Femtosecond-laser-induced nonadiabatic alignment in photoexcited pyrimidine

Shuai Li, Fengzi Ling, Yanmei Wang, Jinyou Long, Xulan Deng, Bing Jin, and Bing Zhang*
State Key Laboratory of Magnetic Resonance and Atomic and Molecular Physics, Wuhan Institute of Physics and Mathematics, Chinese Academy of Sciences, Wuhan 430071, China
and University of Chinese Academy of Sciences, Beijing 100049, China
(Received 21 June 2017; published 29 September 2017)

The rotational wave-packet dynamics in electronically excited pyrimidine induced by a femtosecond laser pulse at 321.5 nm has been studied by time-resolved mass spectroscopy and photoelectron velocity-map imaging. The rotational revival features at 81.3 ps, which are the direct manifestation of field-free nonadiabatic alignment, are clearly observed in both the time-dependent ion yields and photoelectron angular distributions. In particular, the out-of-phase recurrences in the parent-ion and fragment-ions transients indicate the different directions of the ionization transition-dipole moments for the generation of the parent ion and fragment ions. By tuning the polarization of the probe light parallel or perpendicular to that of the pump light, we demonstrate the potential application of nonadiabatic alignment to manipulate the branching ratio of photoionization products.

DOI: 10.1103/PhysRevA.96.033419

I. INTRODUCTION

A linearly polarized laser field can align molecules to given axes fixed in space based on the interaction of the electric dipole with the polarized fields [1–3]. Molecular alignment is emerging as a fascinating problem in fundamental research with a broad range of potential applications ranging from manipulation of chemical reactions [4,5], elucidation of molecular structures [6], tomographic reconstruction of molecular orbitals [7], to fundamental studies in stereochemistry [8], intense laser physics [9,10], high-order-harmonic generation [11,12], surface chemistry [13], coherence and dissipation [14], molecular electronics [15], and new routes to quantum information processing [16]. If the laser pulse duration is shorter than the molecular rotational period, the alignment proceeds nonadiabatically [17] and the field prepares a coherent superposition of rotational eigenstates whose relative phase relations guarantee alignment of the molecular axis with the polarization vector of the laser field. The resulting spatially localized rotational wave packet gives rise to transient alignment due to the dephasing and rephasing of its individual components. As a rapidly progressing approach for manipulating the spatial properties of neutral molecules, nonadiabatic alignment has received a great deal of attention since it opens up the possibility of retaining the alignment after the laser pulse is turned off, i.e., under field-free conditions.

The time-domain approach aimed toward the observation and characterization of alignment effects in various manifestations is known as rotational coherence spectroscopy (RCS) [18,19], which is based on the rotational quantum beats that arise from the coherent excitation of rotational levels within a given vibronic state. The recurrence of an initial spatial anisotropy can be probed in "real time" by a polarization-selective detection process and related to the rotation of the molecular species under study. The majority of the RCS investigations up to date have been performed by means of fluorescence detection [19,20] and photoelectron angular distribution (PAD) measurements [21–23]. However, the method of monitoring the total ion current is problematic since the mixed transition-dipole moment directions arising from ionization to various cationic vibronic levels significantly reduce the observability of rotational coherence effects in the measurement of the total ion current [21]. Thus, it is quite challenging but interesting to observe rotational revivals in the ion transients with mass-selective RCS, i.e., femtosecond time-resolved mass spectroscopy (TR-MS).

In this paper, we utilize such a method to study the dynamics of field-free nonadiabatic alignment in photoexcited pyrimidine and demonstrate the potential application of nonadiabatic alignment to manipulate the branching ratio of photoionization products. Using lasers to control the photoinduced processes in molecules and atoms is a subject of intense activity [24–26]. Of particular interest is controlling the outcome of photochemical reactions in which the reactant molecules yield at least two distinct final products. In general, absorption of polarized light by molecules depends on the alignment of the molecule with respect to the polarization direction [27]. Therefore, by tuning the angle between the pump and probe polarizations, it is possible to preferentially populate a specific ion state, while reducing the population of other ion states. If the ion states are generated by the ionization of various molecular orbitals, they will have different ionization transition-dipole moments. Thus the polarization dependence offers the channel selectivity in the photoionization processes and allows manipulation of the branching ratio of photoionization products.

II. EXPERIMENT

The experiments are performed with the home-built time-of-flight (TOF) mass spectrometer and photoelectron velocity-map imaging spectrometer, which have been described elsewhere [28,29]. Briefly, the vapor of pyrimidine (99% purity) in equilibrium with 2 bars of He was expanded into the vacuum chamber through a 0.5-mm pulsed nozzle, generating a supersonic expansion. The molecular beam was collimated by a 1-mm skimmer and introduced into the interaction region where it was photoexcited and ionized. The resulting ions and photoelectrons were accelerated by the ion lens into

*Corresponding author: bzhang@wipm.ac.cn

a 36-cm field-free region which was shielded against stray magnetic fields by a μ-metal tube and then projected onto a position-sensitive detector consisting of a 40-mm dual-microchannel plate and a phosphor screen (P47). The emission from the phosphor screen was monitored by a photomultiplier connected to a digital phosphor oscilloscope USB interfaced with a computer. The images on the screen were captured with a thermoelectrically cooled charge-coupled device video camera. The observed images of the photoelectrons were inverted using a basis-set expansion (BASEX) transform [30] to calculate the speed and angular distributions.

The seed pulse generated by a commercial Ti:sapphire oscillator was amplified by a chirped pulse regenerative amplifier to deliver a 1 kHz pulse train centered at 797 nm of 100 fs duration with a maximum energy of 4.5 mJ/pulse. The femtosecond pump pulse at 321.5 nm, in resonance with the origin of the first electronically excited singlet state (S_1) at 31 076cm^{-1} [31], was produced by an optical parametric amplifier. The fundamental output at 797 nm served as probe by multiphoton ionization in the TOF measurements, while the frequency-doubled pulse at 398.5 nm was used with two-photon ionization for the photoelectron imaging (PEI) experiments. The pump and probe pulses were weakly focused by a fused silica lens of $f = 400$ mm with the typical energies of $\sim$1 μJ/pulse for the pump pulse, and $\sim$8.6 μJ/pulse (398.5 nm) and $\sim$90 μJ/pulse (797 nm) for the probe pulses, respectively. The time origin ($\Delta t = 0$) of the pump-probe time delay was determined via nonresonant multiphoton ionization of Xe. The laser cross-correlation was also measured by the same method, yielding the values of 146–185 fs, depending on the probe pulse wavelengths. The probe beam was optically delayed with respect to the pump beam by a computer-controlled linear translation stage (PI, M-126.CG1). The polarization of the probe pulse was fixed to be parallel to the detector plane, but the polarization of the pump pulse was accurately controlled by Berek compensators (New Focus).

III. RESULTS AND DISCUSSION

The typical time-of-flight mass spectrum (TOFMS) of pyrimidine obtained at zero delay time following excitation at 321.5 nm and ionization with 797 nm for the parallel pump-probe polarizations, shown in Fig. 1, yields three major mass peaks at $m/z = 80$,53, and 26 amu, respectively; no signals are observed for clusters. It is obvious that the peak at $m/z = 80$ corresponds to the parent ion $C_4H_4N_2^+$. In general, the fragment ions are produced by either direct ionization of the neutral fragments after the dissociation of excited molecules or the dissociative ionization of the parent ion. In the present study, the appearance of fragment ions at $m/z = 53$ and 26 is attributed to the fragmentation processes of the $C_4H_4N_2^+$ parent ion for three major reasons. Firstly, as reported by Lin *et al.* [32] and Yamazaki *et al.* [33], intersystem crossing (ISC) of nanosecond time scale from the S_1 state to the first electronically excited triplet state (T_1) is the dominant process at the low vibrational energy levels of the S_1 state, with a quantum yield of $\sim$1, indicating the absence of the dissociation channel in the relaxation processes around the S_1 origin. Secondly, as described below, the time dependences for

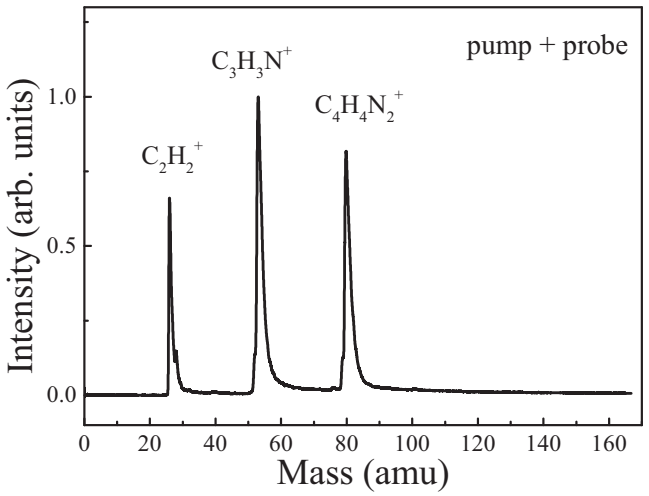

FIG. 1. Mass spectrum of pyrimidine taken at zero delay time between the pump light at 321.5 nm and the probe light at 797 nm.

the two fragment ions at $m/z = 53$ and 26 show a similar decay trend as for the $C_4H_4N_2^+$ parent ion. Thirdly, if the observed fragment ions are from the ionization of the neutral radicals, the time profiles for the two fragment ions should have an additional rising channel, which is not observed in our data fit.

On the basis of the principal fragmentation pathways in the vacuum ultraviolet dissociative photoionization of pyrimidine reported by Leach and co-workers [34], the ion at $m/z = 53$ is assigned to the $C_3H_3N^+$ fragment ion originating from dissociative photoionization associated with the loss of HCN of the $C_4H_4N_2^+$ parent ion. The fragment ion at $m/z = 26$ is attributed to $C_2H_2^+$, presumably formed by the sequential loss of two neutral HCN fragments from the parent ion. The $C_3H_3N^+$ ion is produced in the first step and the acetylene $C_2H_2^+$ ion is produced in the second step. The appearance potentials of the $C_4H_4N_2^+$, $C_3H_3N^+$, and $C_2H_2^+$ ions have been determined to be 9.21, 12.27, and 14.2 eV, respectively [34]. According to the previous studies published by Wolff *et al.* [35], the $C_4H_4N_2^+$ parent ion is formed mostly by the hole in the outermost $7b_2$ valence orbital. The corresponding ion state would then be $1\,^2B_2$, which does not lead to fragmentation. The holes in the molecular orbitals (MOs) $11a_1$, $1a_2$, $10a_1$, and $1b_1$ should be responsible for the formation of the $C_3H_3N^+$ fragment ion. The corresponding ion states would then be $1\,^2A_1$, $1\,^2A_2$, $2\,^2A_1$, and $2\,^2B_1$. However, the specific origin of the $C_3H_3N^+$ fragment ion is not affirmative at present on account of a lack of enough information. The $C_2H_2^+$ fragment ion is likely to originate from the holes in the inner MOs $6b_2$, $9a_1$, $5b_2$, and $8a_1$, corresponding to the $2\,^2B_2$, $3\,^2A_1$, $3\,^2B_2$, and $4\,^2A_1$ ion states, respectively. Due to the existence of the small shoulder at $m/z = 28$ in the observed TOFMS, the origin of the $C_2H_2^+$ fragment ion should include the $3\,^2A_1$ ion state, which is the sole origin for the fragment-ion formation of mass $m/z = 28$ [35]. Thus, it is presumable that the $C_4H_4N_2^+$ parent ion is attributed to the $1\,^2B_2 \leftarrow S_1$ ionization channel, and the $C_2H_2^+$ fragment ion is ascribed to other ionization channels including the $3\,^2A_1 \leftarrow S_1$ transition. It is noted that, for both detection schemes the probe pulse is nonresonant with molecular transitions in the neutral manifold, which has

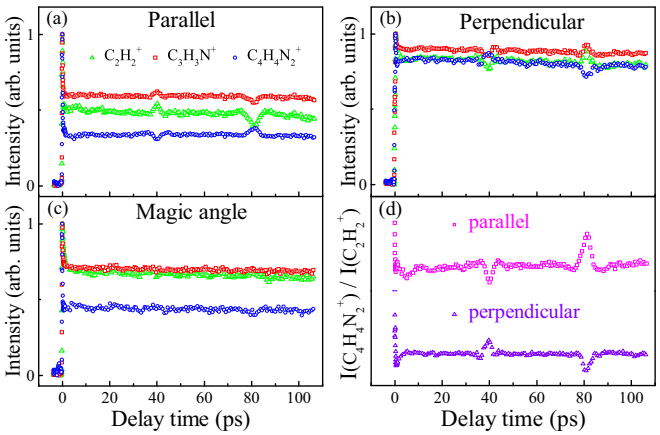

FIG. 2. (a) The temporal profiles obtained by monitoring the ion signals of $C_4H_4N_2^+$ (blue circle), $C_3H_3N^+$ (red square), and $C_2H_2^+$ (green triangle), respectively, when the polarization of the probe light at 797 nm is parallel to that of the pump light at 321.5 nm. The rapid modulations superimposed on the temporal decay profiles are attributed to the rotational wave-packet motion with a full revival time period of 81.3 ps. (b) The time dependences of the intensities for the $C_4H_4N_2^+$ (blue circle), $C_3H_3N^+$ (red square), and $C_2H_2^+$ (green triangle) ions, respectively, obtained for perpendicular relative polarizations. Similar features (initial spike, negative, and positive recurrences) but opposite phases as in Fig. 2(a) are also seen. (c) Time-resolved ion signals of $C_4H_4N_2^+$ (blue circle), $C_3H_3N^+$ (red square), and $C_2H_2^+$ (green triangle), respectively, with the probe polarization set at the magic angle ($\theta = 54.7^\circ$) with respect to the probe polarization. (d) The time-dependent branching ratio of $I(C_4H_4N_2^+)/I(C_2H_2^+)$ obtained for parallel (magenta square) and perpendicular (violet triangle) relative polarizations.

been confirmed by the photoelectron kinetic energy (PKE) distributions measurements.

Figure 2(a) shows the temporal profiles obtained by monitoring the signals of the $C_4H_4N_2^+$, $C_3H_3N^+$, and $C_2H_2^+$ ions, respectively, when the polarization of the probe light at 797 nm is parallel to that of the pump light at 321.5 nm. The time profiles, evidently exhibiting an initial fast decay and a subsequent slow decay, are well fitted by a biexponential decay function convoluted with a Gaussian instrument response function of 146 fs. One decay time τ_1 is 144–156 fs, close to the cross-correlation of pump and probe pulses, and the other decay time τ_2 is of nanosecond time scale that cannot be determined precisely enough with the translation stage used. The time τ_1 represents the nonresonant ionization process occurring only at zero delay time. The long-lived lifetime τ_2, in good agreement with the results reported by the previous spectroscopic studies [33,36], is attributed to the ISC process of the S_1 state.

An interesting issue is that, besides the exponential decay behavior, all of these transients in Fig. 2(a) exhibit the periodic revival structures. The notable and well-resolved features are the sharp spike on the rising edge, and the negative and positive recurrences on the plateaus. These rapid modulations superimposed on the decay profiles are attributed to the rotational wave-packet motion with a full revival time period of 81.3 ps. This spacing compares well with the value estimated from the rotational constants, which have been determined to be $A' = 6352 \pm 3$, $B' = 5853 \pm 3$, and $C' = 3042.0 \pm 0.5$ MHz in the S_1 state [37]. Considering that pyrimidine is an oblate symmetric top molecule, the rotational recurrences occur at times $t = n/(A' + B')$ [38]. The first full revival time ($n = 1$) is estimated to be 81.9 ps, almost precisely equal to the observed value. Note, in particular, while the recurrences in the $C_3H_3N^+$ and $C_2H_2^+$ transients are in phase, the recurrences in the $C_4H_4N_2^+$ parent-ion transient are out of phase with respect to that in the fragment-ion transients. The phases of the modulation indicate the directions of the ion $\leftarrow S_1$ transition-dipole moments. It is presumable that the direction of the ionization transition-dipole moment for the $C_2H_2^+$ fragment ion is the same as that for the $C_3H_3N^+$ ion but different from that for the $C_4H_4N_2^+$ parent ion. Namely, the transition moment for the $1\,^2B_2 \leftarrow S_1$ ionization is quite well approximated as being parallel to the transition moment for the $S_1 \leftarrow S_0$ excitation, but the transition moment for $3\,^2A_1 \leftarrow S_1$ is likely to be perpendicular to the $S_1 \leftarrow S_0$ transition moment.

The sharp features for the perpendicular relative polarizations, shown in Fig. 2(b), are analogous to the recurrences in the parallel relative polarizations, except that the phase (positive/negative) is opposite. That is to say, the phase of the recurrence changes with the relative polarization between the pump and probe pulses. The transients with the probe polarization set at the magic angle with respect to the probe polarization, presented in Fig. 2(c), exhibit an unmodulated population decay signal. The magic angle, $\theta = 54.7^\circ$, is well known as the angle at which to completely eliminate rotational coherence effects in the exponential decays [39]. As described above, the experimentally determined time-dependent ion yield opens a way to access the rotational coherence effects in excited states. Figure 2(d) shows the time-varying branching ratio of $I(C_4H_4N_2^+)/I(C_2H_2^+)$ as a function of time delay. For the parallel relative polarizations, the branching ratio reaches its maximum value of 0.88 at the first full revival time, but for the perpendicular relative polarizations, the branching ratio reaches its minimum value of 0.43 at the first full revival time. That is to say, for the parallel relative polarizations, the photoionization probability of the $1\,^2B_2 \leftarrow S_1$ channel is enhanced at the first full revival time. However, for the perpendicular relative polarizations, the situation is reversed. By virtue of the $C_4H_4N_2^+$ parent ion and the $C_2H_2^+$ fragment ion correlated with the parallel and perpendicular transitions, respectively, the branching ratio of photoionization products can be controlled by tuning the spatial alignment of the pyrimidine molecules with respect to the polarization of the probe light so that either parallel transitions are enhanced and simultaneously perpendicular transitions suppressed or vice versa.

Besides the mass-selective RCS, i.e., femtosecond time-resolved mass spectroscopy, RCS in the form of TR-PEI has proven to be a powerful and valuable approach for an exquisite insight into the dynamic evolution of the coherent rotational wave packet due to the sensitivity of the PADs to the electronic symmetry [21]. To ensure further that the pump pulse at 321.5 nm indeed creates a time-dependent alignment which is applied to manipulate the branching ratio of ion signals, the PAD measurements are made in the $(1+2')$ resonance-enhanced multiphoton ionization scheme of pyrimidine. Figure 3(a) shows the PKE spectrum that is

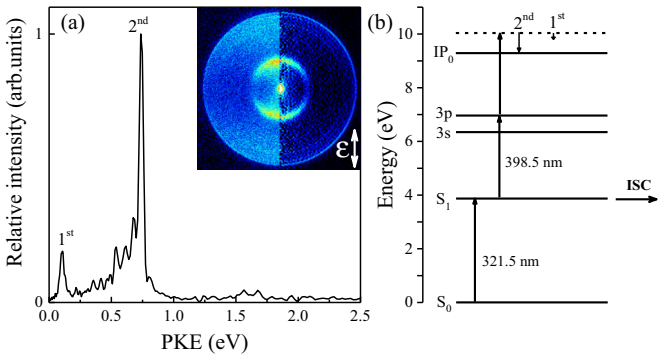

FIG. 3. (a) PKE distribution extracted from the image at $\Delta t = 34.6$ ps. The inset is the corresponding raw photoelectron image. The polarization vectors of both pump and probe laser beams are parallel to each other and in the vertical direction in the figure. (b) A schematic illustration of the (1+2′) resonance-enhanced multiphoton ionization scheme of pyrimidine. The first and second peaks are generated by the accidental resonances with the $3s$ and $3p$ Rydberg states of the S_1 state, respectively.

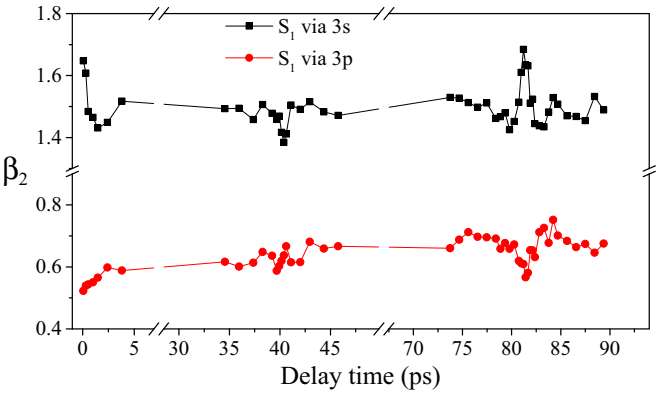

FIG. 4. Time dependences of the β_2 coefficients generated by ionization via the $3s$ (black square) and $3p$ (red circle) Rydberg states extracted from a series of photoelectron images following excitation at 321.5 nm and probing with 398.5 nm. The periodic revival structures are the direct manifestation of the field-free molecular axis alignment created by the pump pulse.

extracted from a typical BASEX-inverted photoelectron image at $\Delta t = 34.6$ ps between the pump pulse at 321.5 nm and the probe pulse at 398.5 nm. The inset is the corresponding raw photoelectron image. Two well-resolved peaks centered at 0.10 and 0.74 eV are observed in the spectrum and marked as the first and second peaks labeled from the inside to outside rings, respectively. The sharp structure indicates that these ionization processes occur via the intermediate Rydberg states. The calculated quantum defects (δ), which can be used to characterize the composition of the Rydberg states, are determined from the observed PKE of 0.10 and 0.74 eV using the formula of PKE $= h\upsilon_{\text{probe}} - R/(n-\delta)^2$ (n denotes the principal quantum number, and R represents the Rydberg constant of 13.606 eV). With suitable n of 3, the δ values are found to be 0.87 and 0.60 for the states associated with the first and second peaks, respectively. Therefore, the states contributing to the two peaks are assigned to the $3s$ and $3p$ Rydberg states, in good agreement with the result reported by Andritsopoulos and co-workers [40]. The energy level diagram is depicted schematically in Fig. 3(b). Pyrimidine is excited to the S_1 state by the pump pulse, and the subsequent 398.5-nm probe pulse is used to probe the wave-packet dynamics by a two-photon process via the Rydberg states.

The distinct anisotropy in the photoelectron image is a valuable supplement for the assignment of the intermediate Rydberg states. The PADs at individual PKEs can be extracted from the observed images. In a cylindrically symmetric system, with the pump and probe laser polarization vectors parallel to each other, the laboratory frame PADs resulting from ionization can be similarly expanded as [41]

$$I(\theta;t) = \sigma(t)[1 + \beta_2(t)P_2(\cos\theta) + \beta_4(t)P_4(\cos\theta) + \beta_6(t)P_6(\cos\theta)], \quad (1)$$

where θ is the angle between the laser polarization direction and the electron recoil direction, $\sigma(t)$ is the integral cross section, $\beta_n(t)$ are the anisotropy parameters, and $P_n(\cos\theta)$ are the Legendre polynomials. In general, the PAD is expected to be more anisotropic in ionization from an s Rydberg state than from a p state. The large anisotropy parameter ($\beta_2 = 1.5$) of the first peak and the smaller parameter ($\beta_2 = 0.6$) of the second peak support our assignment of their electron orbital angular momentum.

Figure 4 shows the time dependences of the β_2 coefficients extracted from a series of photoelectron images following ionization of the S_1 state via the $3s$ and $3p$ Rydberg states, respectively. It is obvious that both of the transients exhibit periodic revival structures due to the rotational wave-packet dynamics, confirming that the pump pulse at 321.5 nm indeed creates a time-varying alignment in the S_1 state at $\Delta t = 0$. The peak position of the rotational recurrence is at 81.4 ps, well in accord with the measurements of ion yields shown in Fig. 2(a). It is noted that the rotational wave-packet modulations in the anisotropy parameters of the PADs for ionization via the $3s$ and $3p$ Rydberg states are out of phase with each other. The pump pulse aligns the figure axis of pyrimidine predominantly parallel to the pump laser polarization. Immediately following one-photon excitation, the system maximally aligns the transition-dipole moment to the pump laser polarization with a $\cos^2\theta$ distribution [21]. Then it can be estimated that about 32.6% of all the molecules have their axis located within the range of $\pm 15°$ with respect to the pump laser polarization, or in another point of view, the degree of alignment $\langle\cos^2\theta\rangle$ is 0.6, which roughly reflects the quality of the rotational wave packet created initially in S_1. In our supersonic beam experiments, rotational decoherence could be caused by (i) collisions between molecules; (ii) absorption or emission of microwave photons; and (iii) the decay of the S_1 state. Neither (i) nor (ii) is relevant within the 1-ns time window [42], and the lifetime near the S_1 origin in pyrimidine is estimated to be about nanosecond scale by the picosecond-resolved fluorescence measurements [33]. Everything mentioned above indicates the slow rate of the rotational decoherence process. Therefore, we speculate that the degree of the alignment is not obviously decreased within several revivals. Indeed a clear revival feature is observed at the first revival time in our data. Since photoionization with the transition dipole either parallel or perpendicular to the molecular figure axis gives rise to a

different composition of the outgoing electron partial waves, the PADs vary with the axis alignment in the Rydberg state at the moment of ionization. However, as the time evolution in the Rydberg state is negligible within the femtosecond pulse, the rotational motion in the Rydberg state during the interaction with a probe laser field can be neglected, and thus the PAD is modulated only by the time dependence of alignment in the S_1 state. The recurrence features are the direct manifestation of the rotational coherence effects in photoexcited pyrimidine. It is noted that the time dependence of the β_2 coefficient via the $3p$ state has a positive slope during the first 45 ps, while this is not present on the other curve. One possible explanation is that the slope is caused by the time evolution of the rotational wave packet, but the differences in the vibrational energy and symmetry between the $3s$ and $3p$ Rydberg states lead to distinct behaviors. The detailed analysis will require more extensive experimental and theoretical investigations.

IV. CONCLUSIONS

In summary, the rotational coherence effect in photoexcited pyrimidine is visualized using the RCS in the forms of femtosecond time-resolved mass spectroscopy and time-resolved photoelectron velocity-map imaging. Field-free nonadiabatic alignment in S_1 pyrimidine is clearly seen as rapid modulations with an internal of 81.3 ps in the time dependences of the ion yields and PADs. In particular, the recurrences in the parent-ion transient are out of phase with respect to that in the fragment-ions transients, indicating that the parent ion and the fragment ions are correlated with the parallel and perpendicular transitions, respectively. Thus, the branching ratio of photoionization products can be controlled by tuning the relative polarizations of the pump and probe laser pulses so that either parallel transitions are enhanced and simultaneously perpendicular transitions suppressed or vice versa. Such an experiment suggests a potential method of the coherent control of wave-packet dynamics. Our results not only demonstrate the promising routes toward the real-time visualization of aligned rotational wave-packet motion in excited states, but also would be quite significant to relevant studies of the steric effects in chemical reaction dynamics.

ACKNOWLEDGMENTS

We gratefully acknowledge financial support from the National Basic Research Program of China (973 Program, Grant No. 2013CB922200) and National Natural Science Foundation of China (Grants No. 91121006, No. 21327804, No. 21573279, No. 21303255, No. Y6S0011037, No. 21503270, No. 11674355, and No. 11574351).

[1] B. Friedrich and D. Herschbach, Phys. Rev. Lett. **74**, 4623 (1995).
[2] E. Péronne, M. D. Poulsen, C. Z. Bisgaard, H. Stapelfeldt, and T. Seideman, Phys. Rev. Lett. **91**, 043003 (2003).
[3] T. Seideman, Phys. Rev. Lett. **83**, 4971 (1999).
[4] T. Seideman, Phys. Rev. A **64**, 042504 (2001).
[5] J. J. Larsen, I. Wendt-Larsen, and H. Stapelfeldt, Phys. Rev. Lett. **83**, 1123 (1999).
[6] M. F. Gelin, C. Riehn, V. V. Matylitsky, and B. Brutschy, Chem. Phys. **290**, 307 (2003).
[7] S. Patchkovskii, Z. X. Zhao, T. Brabec, and D. M. Villeneuve, J. Chem. Phys. **126**, 114306 (2007).
[8] T. P. Rakitzis, A. J. van den Brom, and M. H. M. Janssen, Science **303**, 1852 (2004).
[9] V. R. Bhardwaj, D. Mathur, and F. A. Rajgara. Phys. Rev. Lett. **80**, 3220 (1998).
[10] L. J. Frasinski, J. Plumridge, J. H. Posthumus, K. Codling, P. F. Taday, E. J. Divall, and A. J. Langley, Phys. Rev. Lett. **86**, 2541 (2001).
[11] C. Vozzi, F. Calegari, E. Benedetti, J.-P. Caumes, G. Sansone, S. Stagira, M. Nisoli, R. Torres, E. Heesel, N. Kajumba, J. P. Marangos, C. Altucci, and R. Velotta, Phys. Rev. Lett. **95**, 153902 (2005).
[12] T. Kanai, S. Minemoto, and H. Sakai, Nature (London) **435**, 470 (2005).
[13] V. A. Cho and R. B. Bernstein, J. Phys. Chem. **95**, 8129 (1991).
[14] S. Ramakrishna and T. Seideman, Phys. Rev. Lett. **95**, 113001 (2005).
[15] M. G. Reuter, M. Sukharev, and T. Seideman, Phys. Rev. Lett. **101**, 208303 (2008).
[16] K. F. Lee, D. M. Villeneuve, P. B. Corkum, and E. A. Shapiro, Phys. Rev. Lett. **93**, 233601 (2004).
[17] T. Seideman and E. Hamilton, Adv. At., Mol. Opt. Phys. **52**, 289 (2005).
[18] P. M. Felker, J. Phys. Chem. **96**, 7844 (1992).
[19] J. S. Baskin, P. M. Felker, and A. H. Zewail, J. Chem. Phys. **86**, 2483 (1987).
[20] J. S. Baskin, P. M. Felker, and A. H. Zewail, J. Chem. Phys. **84**, 4708 (1986).
[21] M. Tsubouchi, B. J. Whitaker, L. Wang, H. Kohguchi, and T. Suzuki, Phys. Rev. Lett. **86**, 4500 (2001).
[22] K. L. Reid, T. A. Field, M. Towrie, and P. Matousek, J. Chem. Phys. **111**, 1438 (1999).
[23] C. Qin, Y. Liu, S. Zhang, Y. Wang, Y. Tang, and B. Zhang, Phys. Rev. A **83**, 033423 (2011).
[24] B. Sussman, D. Townsend, M. Ivanov, and A. Stolow, Science **314**, 278 (2006).
[25] R. J. Gordon and S. A. Rice, Annu. Rev. Phys. Chem. **48**, 601 (1997).
[26] R. N. Zare, Science **279**, 1875 (1998).
[27] M. D. Poulsen, E. Skovsen, and H. Stapelfeldt, J. Chem. Phys. **117**, 2097 (2002).
[28] F. Ling, S. Li, X. Song, Y. Tang, Y. Wang, and B. Zhang, Phys. Rev. A **95**, 043421 (2017).
[29] Y. Liu, B. Tang, H. Shen, S. Zhang, and B. Zhang, Opt. Express **18**, 5791 (2010).
[30] V. Dribinski, A. Ossadtchi, V. A. Mandelshtam, and H. Reisler, Rev. Sci. Instrum. **73**, 2634 (2002).
[31] M. Riese and J. Grotemeyer, Anal. Bioanal. Chem. **386**, 59 (2006).
[32] M.-F. Lin, Y. A. Dyakov, C.-M. Tseng, A. M. Mebel, S. H. Lin, Y. T. Lee, and C.-K. Ni, J. Chem. Phys. **124**, 084303 (2006).
[33] I. Yamazaki, T. Murao, T. Yamanaka, and K. Yoshihara, Faraday Discuss. Chem. Soc. **75**, 395 (1983).

[34] M. Schwell, H.-W. Jochims, H. Baumgärtel, and S. Leach, Chem. Phys. **353**, 145 (2008).
[35] W. Wolff, H. Luna, L. Sigaud, A. C. Tavares, and E. C. Montenegro, J. Chem. Phys. **140**, 064309 (2014).
[36] Y. Matsumoto, S. K. Kim, and T. Suzuki, J. Chem. Phys. **119**, 300 (2003).
[37] J. A. Konings, W. A. Majewski, Y. Matsumoto, D. W. Pratt, and W. Leo Meerts, J. Chem. Phys. **89**, 1813 (1988).
[38] P. M. Felker and A. H. Zewail, *Jet Spectroscopy and Molecular Dynamics* (Springer, New York, 1995), p. 181.
[39] K. L. Reid, Annu. Rev. Phys. Chem. **54**, 397 (2003).
[40] A. Bolovinos, P. Tsekeris, J. Philis, E. Pantos, and G. Andritsopoulos, J. Mol. Spectrosc. **103**, 240 (1984).
[41] C. N. Yang, Phys. Rev. **74**, 764 (1948).
[42] A. Przystawik, A. Kickermann, A. Al-Shemmary, S. Düsterer, A. M. Ellis, K. von Haeften, M. Harmand, S. Ramakrishna, H. Redlin, L. Schroedter, M. Schulz, T. Seideman, N. Stojanovic, J. Szekely, F. Tavella, S. Toleikis, and T. Laarmann, Phys. Rev. A **85**, 052503 (2012).